Non-Hermitian topological systems with eigenvalues that are always real

Yang Long, Haoran Xue, and Baile Zhang*

Division of Physics and Applied Physics, School of Physical and Mathematical Sciences, Nanyang Technological University,
21 Nanyang Link, Singapore 637371, Singapore

The effect of non-Hermiticity in band topology has sparked many discussions on non-Hermitian topological physics. It has long been known that non-Hermitian Hamiltonians can exhibit real energy spectra under the condition of parity-time (PT) symmetry—commonly implemented with balanced loss and gain—but only when non-Hermiticity is relatively weak. Sufficiently strong non-Hermiticity, on the other hand, will destroy the reality of energy spectra, a situation known as spontaneous PT-symmetry breaking. Here, based on nonreciprocal coupling, we show a systematic strategy to construct non-Hermitian topological systems exhibiting bulk and boundary energy spectra that are always real, regardless of weak or strong non-Hermiticity. Such nonreciprocal-coupling-based non-Hermiticity can directly drive a topological phase transition and determine the band topology, as demonstrated in a few non-Hermitian systems from one dimensional to two dimensional. Our work develops a theory that can guarantee the reality of energy spectra for non-Hermitian Hamiltonians, and offers an avenue to explore non-Hermitian topological physics.

Conservation of energy in quantum physics demands real eigenenergies for a closed system that is described by a Hermitian Hamiltonian. In the presence of energy exchange with the surrounding environment, the energy conservation is broken. In such a situation, a non-Hermitian Hamiltonian will arise, leading to complex eigenvalues. However, the non-Hermiticity is not a sufficient condition for the existence of complex spectra, which means that it is possible to find a non-Hermitian system with real eigenvalues.

Parity-time (PT) symmetry, one of the major discoveries in non-Hermitian quantum physics, claims that a class of non-Hermitian Hamiltonians with PT symmetry can still have real spectra [1,2]. This counterintuitive discovery fundamentally overturned the past perception that only Hermitian operators can have real eigenvalues. However, the PT-symmetry approach has a long-lasting limitation: it takes effect only when the non-Hermiticity is relatively weak [2–6]; in other words, sufficiently strong non-Hermiticity will destroy the reality of energy spectra even when PT symmetry is still respected— a situation known as spontaneous PT-symmetry breaking [2,7–11]. Therefore, the PT symmetry cannot guarantee the reality of energy spectra. A PT-symmetric Hamiltonian belongs to a more general class of non-Hermitian Hamiltonians known as pseudo-Hermitian Hamiltonians [12,13], but pseudo-Hermiticity does not guarantee the reality of energy spectra either. For example, let us consider $H = i\sigma_z$, which is pseudo-Hermitian since $H^\dagger = \eta H \eta^{-1}$, where $\eta = \sigma_x$, but H has complex eigenvalues of $\pm i$. To our knowledge, there is no theory so far that can guarantee the reality of energy spectra in non-Hermitian systems.

Recently, there have been a lot of efforts in constructing topological states in non-Hermitian systems [14–17]. This combination of topological physics and non-Hermitian physics challenges the conventional understanding of topological phases [18–30], as they were previously defined and classified based on their Hermitian Hamiltonians [31,32]. As a result, there have been many developments for non-Hermitian topological invariants to characterize non-Hermitian topology [3,21–23,33,34]. Another challenge that is still under active exploration is whether the non-Hermitian topological systems can exhibit real energy spectra. Most studies along this line have adopted the PT symmetry in order to maintain the real spectra as much as possible [35–38]. However, all these systems will necessarily exhibit complex spectra in the presence of sufficiently strong non-Hermiticity. Moreover, the nontrivial topology in non-Hermitian topological systems is not necessarily determined by Hermitian parameters [21,22,39–41], but can also be induced directly by non-Hermiticity. For example, recent studies have shown that by introducing deliberately designed loss and gain, a topological phase transition can be induced to generate topological states in non-Hermitian systems [4,11,42–44]. Nonreciprocal coupling is another form of non-Hermiticity, but discussions on its directly induced topological phase transition [e.g., to induce a one-dimensional (1D) nontrivial Zak phase] have been relatively few.

In this Letter we develop an approach to construct non-Hermitian topological systems whose energy spectra are always real, regardless of weak or strong non-Hermiticity. Due to the always real energy spectra, the constructed non-Hermitian systems will not exhibit winding topology in the complex energy plane [14,20], as in the recently discovered skin effect [18,19,21], but will have nontrivial topology defined in momentum space. In particular, the nontrivial topology can be either inherited from the Hermitian counterpart,

*Corresponding author: blzhang@ntu.edu.sg

or induced by non-Hermiticity directly. The approach is developed by the noncommutative matrix production between a nonuniform diagonal matrix and a Hermitian Hamiltonian matrix. The resultant non-Hermitian systems can be implemented with nonreciprocal coupling. We demonstrate the effectiveness of this approach in several concrete examples. In a 1D non-Hermitian system we show that the band topology characterized by Zak phase can be inherited from the Hermitian Su-Schrieffer-Heeger (SSH) model, or induced by the non-Hermiticity. Starting with a two-dimensional (2D) C_3-symmetric Hermitian system that is topologically trivial, we show that the nonzero topological polarization and fractional charges can emerge after introducing non-Hermitian terms, leading to topological corner states. All these examples exhibit real energy spectra for both bulk and boundary states, even in the presence of strong non-Hermiticity.

Let us consider the following equation, which is commonly studied in the regular Sturm-Liouville theory [45]:

$$H_0 \Psi_n = E_n M \Psi_n, \qquad (1)$$

where H_0 is a Hermitian matrix, M is a real diagonal matrix with diagonal elements $M_{ii} > 0$, and Ψ_n is the column vector. One can obtain the eigenvalues of Eq. (1) by solving $|H_0 - E_n M| = 0$ and E_n will be real ($E_n \in \mathbb{R}$) according to the regular Sturm-Liouville theory [45]. Here we consider $M = \text{diag}[\varepsilon_1, \varepsilon_2, \varepsilon_3 ... \varepsilon_N]$ with $\varepsilon_i > 0$, and its determinant is nonzero (i.e., $|M| \neq 0$) so that M^{-1} exists. Based on these facts, we can construct a system with the Hamiltonian H as

$$H = M^{-1} H_0. \qquad (2)$$

Clearly this new system can have real eigenvalues E_n. However, the Hamiltonian H in Eq. (2) is generally non-Hermitian (i.e., $H \neq H^\dagger$). To understand this non-Hermiticity, after performing the Hermitian operation on H, one can obtain that $H^\dagger = (M^{-1} H_0)^\dagger = H_0 M^{-1}$ and usually $H^\dagger = H_0 M^{-1} \neq M^{-1} H_0 = H$, as a result of the noncommutativity for the matrix production, except for some special cases such as when H_0 is diagonal or the components in M are uniformly identical, namely $M = c\mathbb{I}$, where $\mathbb{I}$ is the identity matrix and c is the arbitrary constant.

Although H in Eq. (2) is non-Hermitian, it can have real eigenvalues, which means that there is no point gap in the band structure but only one special line gap that is perpendicular to the real axis in complex energy plane. Based on this special line gap, it is possible for the non-Hermitian Hamiltonian of Eq. (2) to possess nontrivial topology [14,20]. Interestingly, the topology can be either inherited from a topologically nontrivial H_0, or induced by the M matrix with a trivial H_0.

1D non-Hermitian system from the SSH model. As the first example, we discuss a 1D non-Hermitian system with coupling settings shown in Fig. 1(a), similar to the conventional SSH model [46]. The corresponding Hamiltonian is

$$H = \sum_n t_1 a_n^\dagger b_n + \frac{t_1}{\varepsilon} b_n^\dagger a_n + t_2 a_{n+1}^\dagger b_n + \frac{t_2}{\varepsilon} b_n^\dagger a_{n-1}, \qquad (3)$$

where $t_1 = \kappa_0 \tau$, $t_2 = \kappa_0 (1 - \tau)$, $\tau \in (0, 1)$, and $a^\dagger(a)$ and $b^\dagger(b)$ are the creation (annihilation) operators. It can
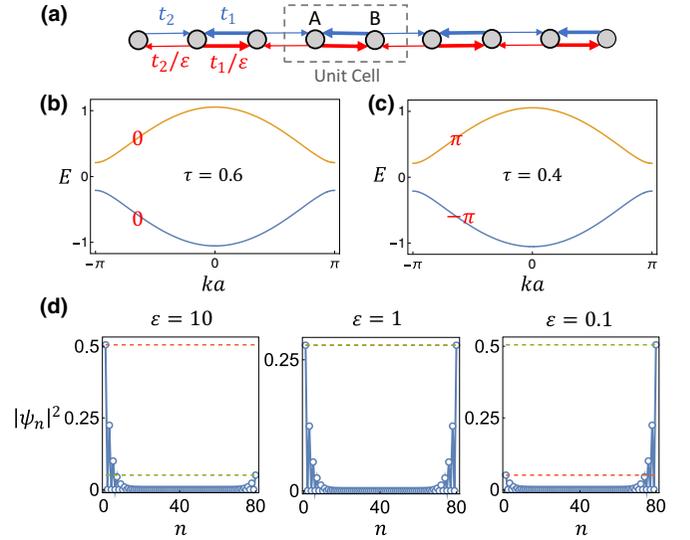
FIG. 1. 1D non-Hermitian topological system with real spectra. (a) System settings. $t_1 = \kappa_0 \tau$ and $t_2 = \kappa_0 (1 - \tau)$, $\kappa_0 = 1$, $\tau \in (0, 1)$, $\varepsilon \in \mathbb{R}$. (b) and (c) Band structures when $\tau = 0.6$ and $\tau = 0.4$. Here $\varepsilon = 0.9$. The red number on each band denotes the Zak phase. (d) The topological edge states will localize toward one end more than the other when $\varepsilon \neq 1$. The system has 80 sites ($N = 80$). The ψ_n denotes the field on the nth site. The blue line with circle markers represents the field distribution. The red and green dotted lines denote the field amplitudes at the left and right ends, respectively.

be regarded as the production of the inverse matrix of $M = \text{diag}[1, \varepsilon, 1, \varepsilon, \dots]$ and the Hamiltonian of the conventional SSH model $H_0 = \sum_n (t_1 b_n^\dagger a_n + t_2 b_n^\dagger a_{n-1} + \text{c.c.})$, namely, $H = M^{-1} H_0$. The Hamiltonian of Eq. (3) in the momentum space can be expressed as

$$H_k = [t_1 + t_2 \cos(ka)] \left(\frac{1 + \varepsilon}{2\varepsilon} \sigma_x + i \frac{\varepsilon - 1}{2\varepsilon} \sigma_y \right)$$
$$+ t_2 \sin(ka) \left(\frac{1 + \varepsilon}{2\varepsilon} \sigma_y - i \frac{\varepsilon - 1}{2\varepsilon} \sigma_x \right), \qquad (4)$$

where k is the Bloch wave vector, a is the lattice constant, and σ_i are the Pauli matrices. This Hamiltonian satisfies the chiral symmetry: $H_k = -\sigma_z H_k \sigma_z$. We can easily obtain its energy spectra: $E_k = \pm \frac{1}{\sqrt{\varepsilon}} \sqrt{t_1^2 + t_2^2 + 2t_1 t_2 \cos(k)}$, as plotted in Figs. 1(b) and 1(c). The spectra are always real even for strong non-Hermiticity (i.e., $\varepsilon \gg 1$ or $\varepsilon \ll 1$). Note that some other non-Hermitian systems based on nonreciprocal couplings, e.g., the Hatano-Nelson model [47], can exhibit real energy spectra under the open boundary condition, but these real spectra are a result of boundary effect, being extremely sensitive to boundary conditions [48–53]. In contrast, the real spectra of our systems are insensitive to boundary conditions. More detailed discussions can be found in the Supplemental Material [54] (see, also, Refs. [55–64] therein).

The topology of our 1D non-Hermitian system can be characterized by the Zak phase: $c_n = -i \int_{-\pi/a}^{\pi/a} \langle w_n | \partial_k | u_n \rangle dk$, where $H_k |u_{k,n}\rangle = E_{k,n} |u_{k,n}\rangle$ and $H_k^\dagger |w_{k,n}\rangle = E_{k,n} |w_{k,n}\rangle$. The Zak phases (c_1, c_2) for the two bands are: $(c_1, c_2) = (0, 0)$ for $t_1 > t_2$ and $(c_1, c_2) = (-\pi, \pi)$ for $t_1 < t_2$ [54,65]. The
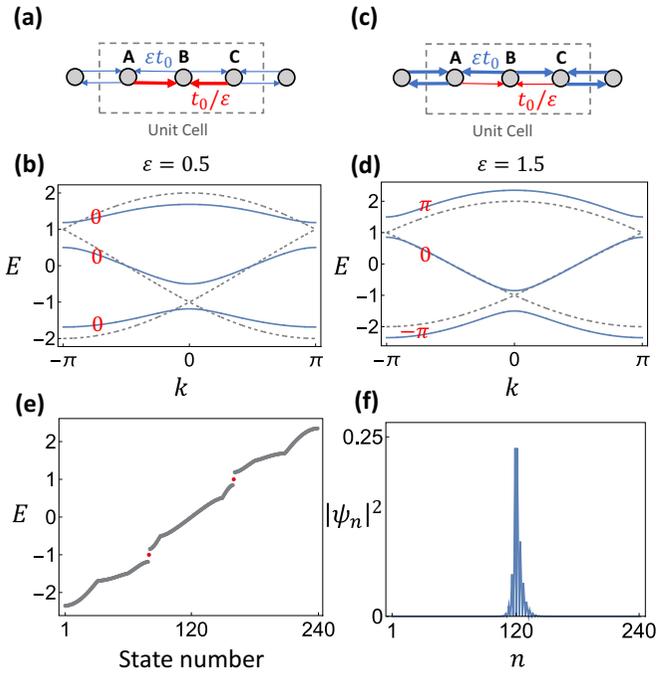
FIG. 2. Non-Hermiticity-induced 1D topological phase transition. (a) The unit cell when $\varepsilon < 1$. The direction and thickness of the arrow represent the coupling direction and strength, respectively. (b) The band structure of a non-Hermitian system ($\varepsilon = 0.5$) with trivial band topology. The red number on each band labels the Zak phase. The blue solid and gray dotted lines denote the band structures with $\varepsilon = 0.5$ and $\varepsilon = 1$, respectively. (c) The unit cell when $\varepsilon > 1$. (d) The band structure of a non-Hermitian system ($\varepsilon = 1.5$) with nontrivial band topology. (e) The topological interface states exist in the bulk gap of the junction system composed of two topologically distinct lattices ($\varepsilon = 0.5$ and $\varepsilon = 1.5$). Each lattice has 120 sites. The interface and bulk states are represented by the red and gray points, respectively. (f) The field distribution of the topological interface state at $E = 1$. The ψ_n denotes the field on the nth site. Here $t_0 = 1$.

nonzero Zak phase for $t_1 < t_2$ indicate that there are two degenerate topological edge states localized at the ends of a finite system, as a manifestation of fractional charges at the ends [66–70]. From Eq. (3) we can see that the mirror symmetry is broken when $\varepsilon \neq 1$. The topological states can be affected by this non-Hermitian parameter. For a finite system with N sites, the ratio between the amplitudes of the left and right edge states is ε [54]: $\frac{|\psi_1|^2}{|\psi_N|^2} = \varepsilon$, where $\psi_{1/N}$ denote the field on the left/right end site. As shown in Fig. 1(d), when $\varepsilon \neq 1$, the topological edge states can localize toward one end more than the other [54].

Non-Hermiticity-induced topological phase transition in 1D system. After demonstrating the topology inherited from the Hermitian topological system H_0 in Eq. (3), we now show that the topology can also be induced by the non-Hermitian parameter ε that is applied to an originally trivial 1D H_0. As shown in Figs. 2(a) and 2(c), the Hamiltonian is

$$H = t_0 \sum_n \frac{1}{\varepsilon} b_n^\dagger a_n + \varepsilon a_n^\dagger b_n + \frac{1}{\varepsilon} b_n^\dagger c_n + \varepsilon c_n^\dagger b_n$$
$$+ \varepsilon(a_{n+1}^\dagger c_n + c_n^\dagger a_{n+1}), \quad (5)$$

which is constructed by a trivial Hermitian system $H_0 = t_0 \sum_n b_n^\dagger a_n + c_n^\dagger b_n + a_{n+1}^\dagger c_n + \text{c.c.}$ and $M = \text{diag}[\varepsilon^{-1}, \varepsilon, \varepsilon^{-1}, \varepsilon^{-1}, \varepsilon, \varepsilon^{-1}, \dots]$, namely, $H = M^{-1}H_0$. The Hamiltonian of Eq. (5) in the momentum space can be written as

$$H_k = t_0 \begin{pmatrix} 0 & \varepsilon & \varepsilon e^{-ika} \\ \frac{1}{\varepsilon} & 0 & \frac{1}{\varepsilon} \\ \varepsilon e^{ika} & \varepsilon & 0 \end{pmatrix}, \quad (6)$$

where k is the wave vector, and a is the lattice constant. Obviously when $\varepsilon = 1$, the H_k represents a gapless Hermitian system. However, after setting $\varepsilon \neq 1$, the spectra of H_k of Eq. (6) can open a gap as presented in Figs. 2(b) and 2(d).

Importantly, when $\varepsilon < 1$ ($\varepsilon > 1$), the system becomes trivial (topological). Compared with the system with $\varepsilon < 1$ in Fig. 2(b), the system with $\varepsilon > 1$, as shown in Fig. 2(d), can lead to the nonzero Zak phases for the first and third bands. After combining the trivial and topological systems into a chain, topological interface states emerge in the bulk gaps, as shown in Figs. 2(e) and 2(f). This shows that the non-Hermitian parameter ε not only makes the H of Eq. (2) become non-Hermitian, but is also able to drive a topological phase transition.

Non-Hermiticity-induced higher-order topological states. We then proceed to demonstrate the non-Hermiticity-induced higher-order topological states in a 2D lattice with C_3 symmetry. The unit cell of the system is shown in Figs. 3(a) and 3(c). When $\varepsilon = 1$, the system corresponds to a trivial C_3-symmetric Hermitian system. The condition of $\varepsilon \neq 1$ cannot only make the system non-Hermitian, but also open a gap at the valley point K, as illustrated in Figs. 3(b) and 3(d) [54]. Notably, the systems with $\varepsilon < 1$ and $\varepsilon > 1$ correspond to trivial and topological ones, respectively.

The higher-order topological properties of the C_3-symmetric non-Hermitian systems can be described by the topological index and symmetry indicator [69,71,72]. The topological index is given by $\chi = ([K_1^{(3)}], [K_2^{(3)}])$, where $[K_1^{(3)}] = \sharp K_1^{(3)} - \sharp \Gamma_1^{(3)}$, $[K_2^{(3)}] = \sharp K_2^{(3)} - \sharp \Gamma_2^{(3)}$ are the symmetry indicators. The $\sharp \Pi_p^{(n)}$ is the number of bands below the band gap with the eigenvalue of C_3 operator $e^{i2\pi(p-1)/n}$ ($p = 1, 2, \dots, n$) at the high-symmetry point $\Pi = \Gamma, K$. We find that $\chi = (-1, 1)$ when $\varepsilon > 1$ and $\chi = (0, 0)$ when $\varepsilon < 1$. Remarkably, the topological bulk polarization $\boldsymbol{P}$ and fractional corner charge Q can be determined by the topological index [69]: $\boldsymbol{P} = (\frac{2}{3}[K_1^{(3)}] + \frac{4}{3}[K_2^{(3)}])(\boldsymbol{a}_1 + \boldsymbol{a}_2) \mod 1$, where $\boldsymbol{a}_{1,2}$ are primitive unit lattice vectors, $Q = \frac{1}{3}[K_2^{(3)}] \mod 1$. When $\varepsilon < 1$, $\boldsymbol{P} = \boldsymbol{0}$ and $Q = 0$. When $\varepsilon > 1$, $\boldsymbol{P} = \frac{2}{3}(\boldsymbol{a}_1 + \boldsymbol{a}_2)$ and $Q = 1/3$. Due to the nonzero $\boldsymbol{P}$ and Q when $\varepsilon > 1$, we can see that there are corner states in the bulk gap for a finite system, as shown in Figs. 3(e) and 3(f).

Non-Hermitian effects on topological edge states in a 2D honeycomb lattice. Here we discuss the non-Hermitian topological valley system in 2D honeycomb lattice, which has the unit cell in Fig. 4(a). The effective non-Hermitian Hamiltonian at the valley point K ($\boldsymbol{k} \rightarrow \boldsymbol{k}_0 + \delta \boldsymbol{k}$, $\boldsymbol{k}_0$ is the wave vector
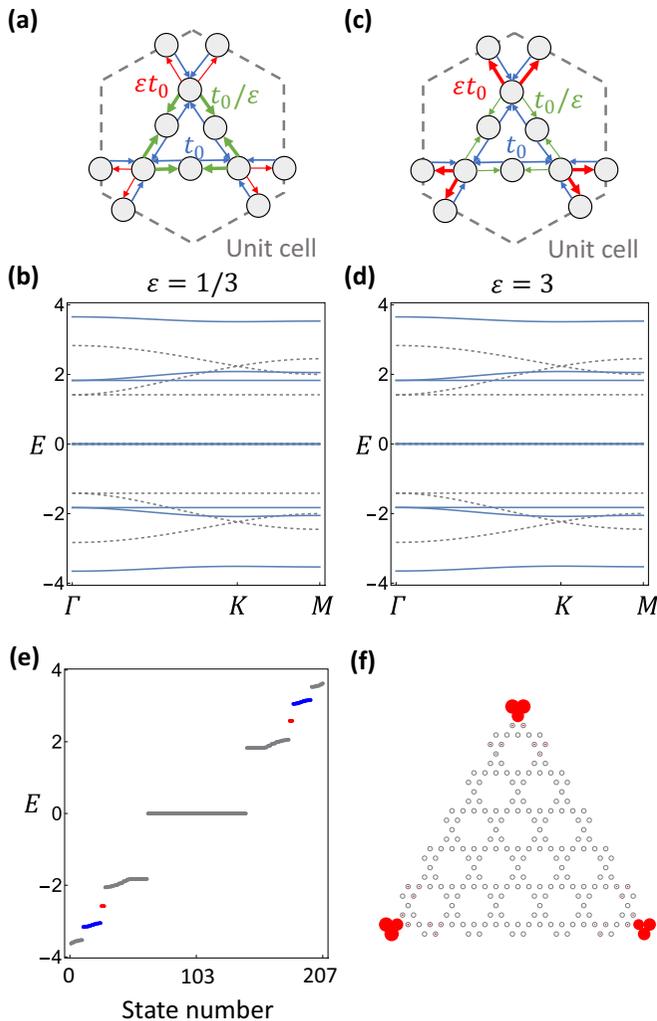
FIG. 3. Non-Hermiticity-induced higher-order topological states in 2D C_3-symmetric lattice. (a) The unit cell when $\varepsilon < 1$, which contains nine sites. (b) The band structure of the non-Hermitian system with $\varepsilon = 1/3$. The blue solid and gray dotted lines denote the band structures with $\varepsilon = 1/3$ and $\varepsilon = 1$, respectively. (c) The unit cell when $\varepsilon > 1$. (d) The band structure of the non-Hermitian system with $\varepsilon = 3$. (e) The eigenvalues for a finite triangular system in (f) with $\varepsilon = 3$. The red, blue, and gray points denote the corner, edge, and bulk states, respectively. (f) The field distribution of topological corner states at $E = -2.58$. The size of red points indicates the field amplitude on the sites. Here $t_0 = 1$.

of K) is [54]

$$
\begin{aligned}
H_k = {} & v_F \delta k_x \left(\frac{1+\varepsilon}{2\varepsilon} \sigma_x + i \frac{\varepsilon-1}{2\varepsilon} \sigma_y \right) \\
& + v_F \delta k_y \left(\frac{1+\varepsilon}{2\varepsilon} \sigma_y - i \frac{\varepsilon-1}{2\varepsilon} \sigma_x \right) + m \sigma_z,
\end{aligned}
\tag{7}
$$

where $\varepsilon \neq 1$, $m_a = -m_b = m$, and $v_F = -\frac{3}{2} t_1 a$, a is the lattice constant. Setting $m \neq 0$ can open a gap at the valley point K/K', as shown in Fig. 4(b). The topological properties of this non-Hermitian valley system can be described by the valley Chern number of the lower band: $C_v = -\frac{\text{sgn}[m]}{2}$ [54,73]. After combining two lattices with different valley Chern numbers
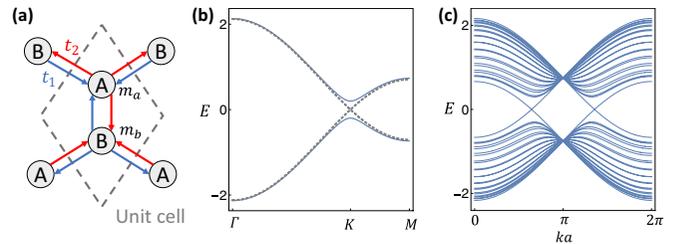
FIG. 4. Non-Hermitian topological valley system. (a) The unit cell of the 2D honeycomb lattice. The t_1 and t_2 are the coupling strengths, $t_2 = \frac{t_1}{\varepsilon}$, $\varepsilon \neq 1$. (b) The band structure of the non-Hermitian system with $\varepsilon = 2.0$. Here $t_1 = -1.0$, $m_a = -m_b = m$. The band structures with $m = 0.2$ and $m = 0$ are represented by the blue solid and gray dashed lines, respectively. (c) The dispersion of the topological edge states on the zigzag interface between two non-Hermitian systems with $m = 0.25$ and $m = -0.25$.

($m > 0$ and $m < 0$) along the zigzag boundary, there are topological edge states existing in the bulk gap [74], as shown in Fig. 4(c). These edge states have the dispersion relation [54]: $E = \pm \frac{v_F}{\sqrt{\varepsilon}} k$, where k is the wave vector of an edge state. This dispersion shows that the ε can affect the propagation velocity of edge states $|v_{\text{edge}}| = |\partial_k E| = \frac{|v_F|}{\sqrt{\varepsilon}}$. When $\varepsilon < 1$ ($\varepsilon > 1$), the propagation velocity of edge states can become faster (slower) than in the Hermitian case: $|v_{\text{edge}}| > |v_F|$ ($|v_{\text{edge}}| < |v_F|$).

Experimental proposals. The non-Hermitian systems shown above can be achieved by electric circuits [75–79]. The electric diode, which makes the electric current flow directionally, can be used to readily establish nonreciprocal coupling [80]. As an example, we demonstrate the circuit realization of a 1D non-Hermitian topological system in Ref. [54]. There are many approaches for classical wave systems to achieve nonreciprocal coupling. For example, the nonreciprocal coupling in optical wave systems can be achieved by exploiting dynamically modulated media [81], metamaterials [82], or S-bending waveguides [83]. For acoustic or elastic wave systems, one can achieve nonreciprocal coupling by using piezophononic media [84], metamaterials [85], or an additional electric setup [17].

To summarize, we propose a systematic strategy to construct real-eigenvalued non-Hermitian topological systems. Compared with previous non-Hermitian systems whose real spectra exist only when non-Hermiticity is relatively weak, our systems exhibit energy spectra that are always real, regardless of weak or strong non-Hermiticity. Furthermore, the nonreciprocal-coupling-based non-Hermiticity is able to affect many properties of topological states. For example, it is able to determine the topology by inducing a topological phase transition. Our work offers an avenue to explore non-Hermitian topological physics [86–90], and would be useful in novel photonic and acoustic devices with nonreciprocal coupling.

[1] C. M. Bender and S. Boettcher, Real Spectra in Non-Hermitian Hamiltonians Having PT Symmetry, Phys. Rev. Lett. **80**, 5243 (1998).

[2] R. El-Ganainy, K. G. Makris, M. Khajavikhan, Z. H. Musslimani, S. Rotter, and D. N. Christodoulides, Non-Hermitian physics and PT symmetry, Nat. Phys. **14**, 11 (2018).

[3] D. Leykam, K. Y. Bliokh, C. Huang, Y. D. Chong, and F. Nori, Edge Modes, Degeneracies, and Topological Numbers in Non-Hermitian Systems, Phys. Rev. Lett. **118**, 040401 (2017).

[4] K. Takata and M. Notomi, Photonic Topological Insulating Phase Induced Solely by Gain and Loss, Phys. Rev. Lett. **121**, 213902 (2018).

[5] A. Y. Song, X.-Q. Sun, A. Dutt, M. Minkov, C. Wojcik, H. Wang, I. A. D. Williamson, M. Orenstein, and S. Fan, PT-Symmetric Topological Edge-Gain Effect, Phys. Rev. Lett. **125**, 033603 (2020).

[6] Y. Ao, X. Hu, Y. You, C. Lu, Y. Fu, X. Wang, and Q. Gong, Topological Phase Transition in the Non-Hermitian Coupled Resonator Array, Phys. Rev. Lett. **125**, 013902 (2020).

[7] C. M. Bender, S. Boettcher, and P. N. Meisinger, PT-symmetric quantum mechanics, J. Math. Phys. **40**, 2201 (1999).

[8] Ş. K. Özdemir, S. Rotter, F. Nori, and L. Yang, Parity–time symmetry and exceptional points in photonics, Nat. Mater. **18**, 783 (2019).

[9] M.-A. Miri and A. Alù, Exceptional points in optics and photonics, Science **363**, eaar7709 (2019).

[10] L. Feng, R. El-Ganainy, and L. Ge, Non-Hermitian photonics based on parity–time symmetry, Nat. Photon. **11**, 752 (2017).

[11] S. Weimann, M. Kremer, Y. Plotnik, Y. Lumer, S. Nolte, K. G. Makris, M. Segev, M. C. Rechtsman, and A. Szameit, Topologically protected bound states in photonic parity–time-symmetric crystals, Nat. Mater. **16**, 433 (2017).

[12] A. Mostafazadeh, Pseudo-Hermiticity versus PT symmetry: The necessary condition for the reality of the spectrum of a non-Hermitian Hamiltonian, J. Math. Phys. **43**, 205 (2002).

[13] R. Zhang, H. Qin, and J. Xiao, PT-symmetry entails pseudo-Hermiticity regardless of diagonalizability, J. Math. Phys. **61**, 012101 (2020).

[14] E. J. Bergholtz, J. C. Budich, and F. K. Kunst, Exceptional topology of non-Hermitian systems, Rev. Mod. Phys. **93**, 015005 (2021).

[15] F. Song, S. Yao, and Z. Wang, Non-Hermitian Skin Effect and Chiral Damping in Open Quantum Systems, Phys. Rev. Lett. **123**, 170401 (2019).

[16] S. Weidemann, M. Kremer, T. Helbig, T. Hofmann, A. Stegmaier, M. Greiter, R. Thomale, and A. Szameit, Topological funneling of light, Science **368**, 311 (2020).

[17] L. Zhang, Y. Yang, Y. Ge, Y.-J. Guan, Q. Chen, Q. Yan, F. Chen, R. Xi, Y. Li, D. Jia, S.-Q. Yuan, H.-X. Sun, H. Chen, and B. Zhang, Acoustic non-Hermitian skin effect from twisted winding topology, Nat. Commun. **12**, 6297 (2021).

[18] T. E. Lee, Anomalous Edge State in a Non-Hermitian Lattice, Phys. Rev. Lett. **116**, 133903 (2016).

[19] Z. Gong, Y. Ashida, K. Kawabata, K. Takasan, S. Higashikawa, and M. Ueda, Topological Phases of Non-Hermitian Systems, Phys. Rev. X **8**, 031079 (2018).

[20] K. Kawabata, K. Shiozaki, M. Ueda, and M. Sato, Symmetry and Topology in Non-Hermitian Physics, Phys. Rev. X **9**, 041015 (2019).

[21] S. Yao and Z. Wang, Edge States and Topological Invariants of Non-Hermitian Systems, Phys. Rev. Lett. **121**, 086803 (2018).

[22] S. Yao, F. Song, and Z. Wang, Non-Hermitian Chern Bands, Phys. Rev. Lett. **121**, 136802 (2018).

[23] F. Song, S. Yao, and Z. Wang, Non-Hermitian Topological Invariants in Real Space, Phys. Rev. Lett. **123**, 246801 (2019).

[24] Y. Yi and Z. Yang, Non-Hermitian Skin Modes Induced by On-Site Dissipations and Chiral Tunneling Effect, Phys. Rev. Lett. **125**, 186802 (2020).

[25] N. Okuma, K. Kawabata, K. Shiozaki, and M. Sato, Topological Origin of Non-Hermitian Skin Effects, Phys. Rev. Lett. **124**, 086801 (2020).

[26] K. Zhang, Z. Yang, and C. Fang, Correspondence between Winding Numbers and Skin Modes in Non-Hermitian Systems, Phys. Rev. Lett. **125**, 126402 (2020).

[27] D. S. Borgnia, A. J. Kruchkov, and R.-J. Slager, Non-Hermitian Boundary Modes and Topology, Phys. Rev. Lett. **124**, 056802 (2020).

[28] T. Yoshida, T. Mizoguchi, and Y. Hatsugai, Mirror skin effect and its electric circuit simulation, Phys. Rev. Research **2**, 022062(R) (2020).

[29] T. Yoshida, R. Peters, N. Kawakami, and Y. Hatsugai, Symmetry-protected exceptional rings in two-dimensional correlated systems with chiral symmetry, Phys. Rev. B **99**, 121101(R) (2019).

[30] T. Isobe, T. Yoshida, and Y. Hatsugai, Topological band theory of a generalized eigenvalue problem with Hermitian matrices: Symmetry-protected exceptional rings with emergent symmetry, Phys. Rev. B **104**, L121105 (2021).

[31] D. Xiao, M.-C. Chang, and Q. Niu, Berry phase effects on electronic properties, Rev. Mod. Phys. **82**, 1959 (2010).

[32] M. Z. Hasan and C. L. Kane, Colloquium: Topological insulators, Rev. Mod. Phys. **82**, 3045 (2010).

[33] H. Shen, B. Zhen, and L. Fu, Topological Band Theory for Non-Hermitian Hamiltonians, Phys. Rev. Lett. **120**, 146402 (2018).

[34] K. Yokomizo and S. Murakami, Non-Bloch Band Theory of Non-Hermitian Systems, Phys. Rev. Lett. **123**, 066404 (2019).

[35] Y. C. Hu and T. L. Hughes, Absence of topological insulator phases in non-Hermitian PT-symmetric Hamiltonians, Phys. Rev. B **84**, 153101 (2011).

[36] M. S. Rudner and L. S. Levitov, Topological Transition in a Non-Hermitian Quantum Walk, Phys. Rev. Lett. **102**, 065703 (2009).

[37] K. Esaki, M. Sato, K. Hasebe, and M. Kohmoto, Edge states and topological phases in non-Hermitian systems, Phys. Rev. B **84**, 205128 (2011).

[38] M. Sato, K. Hasebe, K. Esaki, and M. Kohmoto, Time-reversal symmetry in non-Hermitian systems, Prog. Theor. Phys. **127**, 937 (2012).

[39] K. Kawabata and M. Sato, Real spectra in non-Hermitian topological insulators, Phys. Rev. Research **2**, 033391 (2020).

[40] S. A. A. Ghorashi, T. Li, and M. Sato, Non-Hermitian higher-order Weyl semimetals, Phys. Rev. B **104**, L161117 (2021).

[41] S. A. A. Ghorashi, T. Li, M. Sato, and T. L. Hughes, Non-Hermitian higher-order Dirac semimetals, Phys. Rev. B **104**, L161116 (2021).

[42] H. Xue, Q. Wang, B. Zhang, and Y. D. Chong, Non-Hermitian Dirac Cones, Phys. Rev. Lett. **124**, 236403 (2020).

[43] H. Gao, H. Xue, Z. Gu, T. Liu, J. Zhu, and B. Zhang, Non-Hermitian route to higher-order topology in an acoustic crystal, Nat. Commun. **12**, 1888 (2021).

[44] X.-W. Luo and C. Zhang, Higher-Order Topological Corner States Induced by Gain and Loss, Phys. Rev. Lett. **123**, 073601 (2019).

[45] A. Zettl, *Sturm-Liouville Theory*, 121 (American Mathematical Society, Providence, RI, 2010).

[46] W. P. Su, J. R. Schrieffer, and A. J. Heeger, Solitons in Polyacetylene, Phys. Rev. Lett. **42**, 1698 (1979).

[47] N. Hatano and D. R. Nelson, Localization Transitions in Non-Hermitian Quantum Mechanics, Phys. Rev. Lett. **77**, 570 (1996).

[48] N. Hatano and D. R. Nelson, Vortex pinning and non-Hermitian quantum mechanics, Phys. Rev. B **56**, 8651 (1997).

[49] N. Hatano and D. R. Nelson, Non-Hermitian delocalization and eigenfunctions, Phys. Rev. B **58**, 8384 (1998).

[50] F. K. Kunst, E. Edvardsson, J. C. Budich, and E. J. Bergholtz, Biorthogonal Bulk-Boundary Correspondence in Non-Hermitian Systems, Phys. Rev. Lett. **121**, 026808 (2018).

[51] C. H. Lee and R. Thomale, Anatomy of skin modes and topology in non-Hermitian systems, Phys. Rev. B **99**, 201103(R) (2019).

[52] R. Koch and J. C. Budich, Bulk-boundary correspondence in non-Hermitian systems: Stability analysis for generalized boundary conditions, Eur. Phys. J. D **74**, 70 (2020).

[53] Y. Xiong, Why does bulk boundary correspondence fail in some non-Hermitian topological models, J. Phys. Commun. **2**, 035043 (2018).

[54] See Supplemental Material at http://link.aps.org/supplemental/10.1103/PhysRevB.105.L100102 for more details about the Hamiltonians, the nonsensitivity of our systems to boundary conditions, and the effect of the nondiagonal M, topologically valley-protected edge states, and experimental proposals.

[55] H. Xue, Y. Yang, F. Gao, Y. Chong, and B. Zhang, Acoustic higher-order topological insulator on a kagome lattice, Nat. Mater. **18**, 108 (2019).

[56] X. Ni, M. Weiner, A. Alù, and A. B. Khanikaev, Observation of higher-order topological acoustic states protected by generalized chiral symmetry, Nat. Mater. **18**, 113 (2019).

[57] J. Zeng, H. Liu, H. Jiang, Q.-F. Sun, and X. C. Xie, Multiorbital model reveals a second-order topological insulator in 1H transition metal dichalcogenides, Phys. Rev. B **104**, L161108 (2021).

[58] D. C. Brody, Biorthogonal quantum mechanics, J. Phys. A: Math. Theor. **47**, 035305 (2014).

[59] L. Xiao, K. Wang, X. Zhan, Z. Bian, K. Kawabata, M. Ueda, W. Yi, and P. Xue, Observation of Critical Phenomena in Parity-Time-Symmetric Quantum Dynamics, Phys. Rev. Lett. **123**, 230401 (2019).

[60] K. Kawabata, Y. Ashida, and M. Ueda, Information Retrieval and Criticality in Parity-Time-Symmetric Systems, Phys. Rev. Lett. **119**, 190401 (2017).

[61] A. Regensburger, C. Bersch, M.-A. Miri, G. Onishchukov, D. N. Christodoulides, and U. Peschel, Parity–time synthetic photonic lattices, Nature (London) **488**, 167 (2012).

[62] M. Ezawa, Higher-order topological electric circuits and topological corner resonance on the breathing kagome and pyrochlore lattices, Phys. Rev. B **98**, 201402(R) (2018).

[63] M. Ezawa, Non-Hermitian boundary and interface states in nonreciprocal higher-order topological metals and electrical circuits, Phys. Rev. B **99**, 121411(R) (2019).

[64] J. Ningyuan, C. Owens, A. Sommer, D. Schuster, and J. Simon, Time- and Site-Resolved Dynamics in a Topological Circuit, Phys. Rev. X **5**, 021031 (2015).

[65] J. Zak, Berry's Phase for Energy Bands in Solids, Phys. Rev. Lett. **62**, 2747 (1989).

[66] D. Vanderbilt and R. D. King-Smith, Electric polarization as a bulk quantity and its relation to surface charge, Phys. Rev. B **48**, 4442 (1993).

[67] R. Resta, Macroscopic polarization in crystalline dielectrics: the geometric phase approach, Rev. Mod. Phys. **66**, 899 (1994).

[68] B. Bradlyn, L. Elcoro, J. Cano, M. G. Vergniory, Z. Wang, C. Felser, M. I. Aroyo, and B. A. Bernevig, Topological quantum chemistry, Nature (London) **547**, 298 (2017).

[69] W. A. Benalcazar, T. Li, and T. L. Hughes, Quantization of fractional corner charge in C_n-symmetric higher-order topological crystalline insulators, Phys. Rev. B **99**, 245151 (2019).

[70] W. A. Benalcazar, B. A. Bernevig, and T. L. Hughes, Electric multipole moments, topological multipole moment pumping, and chiral hinge states in crystalline insulators, Phys. Rev. B **96**, 245115 (2017).

[71] Y. Liu, S. Leung, F.-F. Li, Z.-K. Lin, X. Tao, Y. Poo, and J.-H. Jiang, Bulk–disclination correspondence in topological crystalline insulators, Nature (London) **589**, 381 (2021).

[72] R. Okugawa, R. Takahashi, and K. Yokomizo, Non-Hermitian band topology with generalized inversion symmetry, Phys. Rev. B **103**, 205205 (2021).

[73] J. Lu, C. Qiu, L. Ye, X. Fan, M. Ke, F. Zhang, and Z. Liu, Observation of topological valley transport of sound in sonic crystals, Nat. Phys. **13**, 369 (2017).

[74] M. Wang, L. Ye, J. Christensen, and Z. Liu, Valley Physics in Non-Hermitian Artificial Acoustic Boron Nitride, Phys. Rev. Lett. **120**, 246601 (2018).

[75] V. V. Albert, L. I. Glazman, and L. Jiang, Topological Properties of Linear Circuit Lattices, Phys. Rev. Lett. **114**, 173902 (2015).

[76] S. Imhof, C. Berger, F. Bayer, J. Brehm, L. W. Molenkamp, T. Kiessling, F. Schindler, C. H. Lee, M. Greiter, T. Neupert, and R. Thomale, Topolectrical-circuit realization of topological corner modes, Nat. Phys. **14**, 925 (2018).

[77] W. Zhu, Y. Long, H. Chen, and J. Ren, Quantum valley Hall effects and spin-valley locking in topological Kane-Mele circuit networks, Phys. Rev. B **99**, 115410 (2019).

[78] W. Zhu, S. Hou, Y. Long, H. Chen, and J. Ren, Simulating quantum spin Hall effect in the topological Lieb lattice of a linear circuit network, Phys. Rev. B **97**, 075310 (2018).

[79] S. Liu, R. Shao, S. Ma, L. Zhang, O. You, H. Wu, Y. J. Xiang, T. J. Cui, and S. Zhang, Non-Hermitian skin effect in a non-Hermitian electrical circuit, Research **2021**, 5608038 (2021).

[80] M. Ezawa, Non-Hermitian higher-order topological states in nonreciprocal and reciprocal systems with their electric-circuit realization, Phys. Rev. B **99**, 201411(R) (2019).

[81] Z. Yu and S. Fan, Complete optical isolation created by indirect interband photonic transitions, Nat. Photon. **3**, 91 (2009).

[82] D. L. Sounas, C. Caloz, and A. Alù, Giant non-reciprocity at the subwavelength scale using angular momentum-biased metamaterials, Nat. Commun. **4**, 2407 (2013).

[83] Y. G. N. Liu, P. S. Jung, M. Parto, D. N. Christodoulides, and M. Khajavikhan, Gain-induced topological response

via tailored long-range interactions, Nat. Phys. **17**, 704 (2021).

[84] P. Gao, M. Willatzen, and J. Christensen, Anomalous Topological Edge States in Non-Hermitian Piezophononic Media, Phys. Rev. Lett. **125**, 206402 (2020).

[85] B. Liang, X. S. Guo, J. Tu, D. Zhang, and J. C. Cheng, An acoustic rectifier, Nat. Mater. **9**, 989 (2010).

[86] Q.-B. Zeng, Y.-B. Yang, and R. Lü, Topological phases in one-dimensional nonreciprocal superlattices, Phys. Rev. B **101**, 125418 (2020).

[87] T. Liu, Y.-R. Zhang, Q. Ai, Z. Gong, K. Kawabata, M. Ueda, and F. Nori, Second-Order Topological Phases in Non-Hermitian Systems, Phys. Rev. Lett. **122**, 076801 (2019).

[88] C. H. Lee, L. Li, and J. Gong, Hybrid Higher-Order Skin-Topological Modes in Nonreciprocal Systems, Phys. Rev. Lett. **123**, 016805 (2019).

[89] W. Xiong, Z. Li, Y. Song, J. Chen, G.-Q. Zhang, and M. Wang, Higher-order exceptional point in a pseudo-Hermitian cavity optomechanical system, Phys. Rev. A **104**, 063508 (2021).

[90] Q.-B. Zeng, Real spectra, anderson localization, and topological phases in one-dimensional quasireciprocal systems, arXiv:2110.06597.